doi:10.1038/nature09724

Observations and Data Reduction

A summary of the observations used in this work is presented in Supplementary Table 1. A detailed description of the observations is given below.

Near-IR and Optical Imaging with *HST*

High-resolution near-infrared *Hubble Space Telescope* (*HST*) observations of Henize 2-10 were obtained with the Near Infrared Camera and Multiobject Spectrometer (NICMOS) using the NIC 2 Camera. Images through the F187N, F190N, and F205W filters were taken on 2006 October 1. The F187N and F190N narrowband filters cover the Paα hydrogen recombination line (rest wavelength of 1.87μm) and the neighboring continuum, respectively. At the redshift of Henize 2-10 (z = 0.002912), the Paα line falls near the centre and maximum throughput of the F187N filter. The broadband F205W filter ($\sim$ K-band) is centred at approximately 2.1μm. Four dithered sub-exposures were taken in each filter with total on-source integration times of 896 s (F187N), 960 s (F190N) and 480 s (F205W). In addition, off-source observations of equal time were obtained in order to mitigate the effects of the thermal background.

The data were processed following the procedure outlined in Reines et al. (2008b)[19]. The final images have a plate scale of $\sim$0.″0375 pixel^{-1} and are essentially diffraction limited with spatial resolutions of $\sim$0.″2. The F187N and F190N images were used to construct a continuum-subtracted Paα flux image. The image units of DN s^{-1} were converted to flux densities using the inverse sensitivity PHOTFLAM header keywords. The continuum image (F190N) was then subtracted from the line image (F187N), which in turn was multiplied by the width of the F187N filter.

In addition to the new NICMOS observations presented here, we also utilize archival optical observations of Henize 2-10. Images through the F814W ($\sim$ I-band, 0.8 μm) and F330W ($\sim$ U-band, 0.3 μm) filters were obtained with the Advanced Camera for Surveys (ACS) High Resolution Channel (HRC) on 2006 March 12 under Proposal ID 10609 (W. Vacca). We retrieved the pipeline-produced, calibrated and drizzled images from the *HST* archive. The HRC has a plate scale of $\sim$0.″027 pixel^{-1} and the resolution of the images of Henize 2-10 are in the range $\sim$0.″06 - 0.″08. We also obtained archival narrowband images of Henize 2-10 taken through an Hα filter. The observations were taken on 1997 April 3 with the Wide Field and Planetary Camera 2 (WFPC2) under Proposal ID 6580 (P. Conti). The F658N filter was used and the galaxy was placed on the PC chip with a plate scale of $\sim$0.″05 pixel^{-1}. We combined four pipeline-produced calibrated sub-exposures and rejected cosmic rays using custom IDL programs. The final F658N image has a resolution of $\sim$0.″13. Since no narrowband continuum image was available for subtraction, the F658N image contains both line and continuum emission.

Radio Continuum Observations with the VLA

We obtained new X-band (8.5 GHz, 3.5 cm) and C-band (4.9 GHz, 6.2 cm) observations of

Henize 2-10 in December of 2004 with the Very Large Array (VLA)*. These observations were taken in the A-array and utilized the the link to the Pie Town Antenna in the Very Long Baseline Array, resulting in an increased spatial resolution roughly a factor of two better than possible with the VLA alone. The resulting data are the highest resolution and most sensitive VLA observations of Henize 2-10 available to date.

The data were calibrated using the Astronomical Image Processing System (AIPS) software package. The flux density scale was calibrated using the standard sources 0713+438 and 3C286 for both the 3.5 cm and 6.2 cm data. The target and phase calibrator (0836-202) were observed using "fast switching mode" at both frequencies: for the 3.5 cm data, the phase calibrator was observed for 2 minutes before and after every 10 minutes on Henize 2-10, and for the 6.2 cm data the phase calibrator was observed for 2 minutes before and after every 14 minutes observing Henize 2-10. A total of ~ 4 hours and ~ 5 hours of integration time were spent on Henize 2-10 at 3.5 cm and 6.2 cm, respectively.

Given the nature of interferometric observations, it is not possible to obtain identical $u-v$ coverage at each wavelength. However, in order to obtain images at each wavelength with well-matched spatial sensitivity, we endeavor to attain relatively well matched synthesized beams using three steps: first, the uv-range of the observations is restricted to values greater that 6.5 kλ at each wavelength, which will result in approximately similar sensitivity to large spatial scales; second, we vary the weighting used in the imaging process via the "robust" parameter (robust = 5 invokes purely natural weighting, while a robust = -5 invokes purely uniform weighting); and third, the resulting images are convolved to identical resolution elements. The resulting 3.5 cm image was created using robust=5 and the 6.2 cm image with robust = -1, which resulted in synthesized beams of $0\farcs44 \times 0\farcs21$ and $0\farcs55 \times 0\farcs15$, respectively. The final images were convolved to $0\farcs55 \times 0\farcs21$, which corresponds to a FWHM of ~ 24 pc$\times$9 pc at the distance of Henize 2-10. At this resolution, the central source in Henize 2-10 is consistent with being point-like.

We also re-reduced and analyzed existing archival radio observations of Henize 2-10 for comparison. In this process, we found that the 6.2 cm data reported in Johnson & Kobulnicky (2003)[9] that was observed in 1995 had flux densities about half those of the new data for all of the compact sources in Henize 2-10. This discrepancy is likely due to the 1995 data having being taken during poor atmospheric conditions, which resulted in significant decorrelation of the signal, and hence low flux densities. Consequently, we have opted to exclude the 1995 data from the analysis presented in this paper.

Flux densities were measured using the VIEWER program in the CASA software package. Identical apertures were used at each wavelength with an area of approximately twice the size of the synthesized beam (resulting in an ellipse of $\sim 1'' \times 0\farcs5$). Given the substantial diffuse emission

*The National Radio Astronomy Observatory is a facility of the National Science Foundation operated under cooperative agreement by Associated Universities, Inc.

in the area, background estimates were also made using the source-free areas to the north and south of the central object, and the background values were subtracted from the source aperture flux density to obtain the final values of 1.25 mJy and 1.55 mJy at 3.5 cm and 6.2 cm, respectively. We estimate the uncertainty in the relative flux densities to be $\sim 10-20\%$ based on the absolute flux calibration.

Chandra X-ray Data

Henize 2-10 was observed for 19755 s with the Advanced CCD Imaging Spectrometer (ACIS) detector of the *Chandra X-ray Observatory* (CXO) on 2001 March 23 (Observation 2075). Although previous analyses have discussed the diffuse gas and the central source of Henize 2-10 revealed in X-rays[10,31], we undertook an independent analysis of the X-ray point sources to verify the association of the central source with the non-thermal radio source and determine its X-ray properties. Our primary analysis used CIAO 4.1[32] with CALDB 4.1.1 and NASA's HEASOFT 6.6.2[†].

Throughout the observation, Henize 2-10 was located on the ACIS-7 (S3) chip and no background flares were observed. To detect X-ray point sources, we supplied the CIAO WAVDETECT routine with an image of the S3 chip over the 0.3–6 keV range and a mono-energetic exposure map at 1 keV. We used this wavelet detection algorithm to identify sources with $\sqrt{2}$ scales ranging from 1 to 32 pixels ($\sim 0.''5$–$16''$) with a source detection threshold of 10^{-6}. We detected 35 X-ray point sources, while only expecting $\lesssim 1$ false source due to a statistical fluctuation in the background.

Since CIAO WAVDETECT does not take into account the shape of the X-ray PSF, we refined the source positions using ACIS Extract 2009-01-27[33]. For each source, we also used ACIS Extract to create a source extraction region set to encircle 90% of the flux in the X-ray PSF, as well as a circular masking region and a local background region. We then estimated the statistical error in the position using the net counts for each source[34].

The central X-ray source in Henize 2-10 is associated with the non-thermal radio source (see below), and we hereafter only consider this X-ray source with ~ 180 net counts. We extracted spectra for the source and its background in the 0.5–10 keV range (Supplementary Figure 1) . The source spectrum was grouped to have 16 counts per bin, and all spectra were fitted using the Cash statistic[35]. As noted previously[10,31], the source emission has peaks at both soft energies ($\lesssim 1$ keV) and hard energies (~ 3 keV). The peak at hard X-ray emission likely points to a non-thermal process that is moderately affected by absorption. Since the source lies near the peak of the diffuse interstellar medium in Henize 2-10[10], some of its soft energy counts may arise from diffuse gas that undergoes weaker absorption, even after the subtraction of a local background. Alternatively, the soft emission could be intrinsic to the source; however, for most spectral models the observed spectral shape implies that there must be different absorption column densities for the soft and hard components. All models were fit to spectra of the source and nearby backgrounds using XSPEC

[†]See http://heasarc.gsfc.nasa.gov/docs/software/lheasoft/.

12.5.

For our fiducial source model, we assumed the spectrum was due to a combination of absorbed diffuse gas and an absorbed power-law, $\mathrm{tbabs_{Gal}} * (\mathrm{tbabs_{ISM}} * \mathrm{vmekal_{ISM}} + \mathrm{tbabs_{pow}} * \mathrm{pow})$. We adopted updated abundances and photoelectric absorption cross-sections[36,37] for use with the Tuebingen-Boulder ISM absorption model (tbabs). The power-law spectra, $N(E) \propto E^{-\Gamma}$, is what one might expect from a hard-state X-ray binary or an active galactic nucleus; similar spectra have also been used to model supernova remnants like the Crab nebula. To model the contribution from diffuse gas, we adopted a fit to the diffuse gas of the entire galaxy by Kobulnicky & Martin (2010)[10], an optically thin thermal plasma model (0.64 keV) with independent abundances of α (0.77 Solar) and Fe-peak (0.29 Solar) elements (i.e., a vmekal model).

Since the diffuse gas fit from the literature was over a large region of the galaxy and used the wabs absorption model, the absorption column density near the source may differ. We therefore first fit this model to spectra extracted from a region within $\sim 5''$ of the central source, excluding the masking regions of all sources and allowing the model normalization and local absorption along the line-of sight to vary. This led to a larger absorption ($N_{H,\mathrm{ISM}} = 1.3 \times 10^{21}$ cm^{-2} on top of $N_{H,\mathrm{Gal}}$[38] $\equiv 9.7 \times 10^{20}$ cm^{-2}) than reported in Kobulnicky & Martin (2010)[10]. We adopted our larger absorption column densities, but allowed the normalization to vary for modeling the excess ISM inside the source extraction region.

The best-fit model found $N_{H,\mathrm{pow}} = (6.3^{+5.5}_{-3.6}) \times 10^{22}$ cm^{-2} and $\Gamma_{\mathrm{pow}} = 1.66^{+1.16}_{-0.85}$ with a C-statistic of 7.34 for 8 degrees of freedom; the errors reported represent 90% confidence intervals. Since $\sim 16\%$ of realization simulated from the best fit have a lower C-statistic, this suggests the model is an acceptable fit. We note that the normalization of the vmekal model is consistent with expectations for excess diffuse ISM in the source extraction region. To avoid difficulties accounting for the moderately strong absorption at soft energies, as well as placing this source on the fundamental plane of black hole activity, we calculated the observed fluxes and intrinsic luminosities in the 2–10 keV band. Correcting for the encircled energy of the source extraction regions, the observed fluxes from models within the confidence interval are $1.7\text{–}2.6 \times 10^{-13}$ erg cm^{-2} s^{-1}, with a best-fit flux of 2.1×10^{-13} erg cm^{-2} s^{-1}. We note that our lowest flux is consistent with that derived by Kobulnicky & Martin (2010)[10]. After removing Galactic and local absorption, the intrinsic luminosities range from $2.7\text{–}3.5 \times 10^{39}$ erg s^{-1}, with a best-fit luminosity of 2.7×10^{39} erg s^{-1}.

To verify that these numbers are not biased by our choice of fiducial spectra, we tried a variety of other plausible models that might arise from X-ray binaries, active galactic nuclei, supernova remnants, or young supernovae. While the current spectra are not sufficiently accurate to pinpoint the spectral components, they do produce a consistent flux and intrinsic luminosity in the hard 2–10 keV band.

Astrometry

To facilitate the comparison of multi-wavelength observations of Henize 2-10, we registered

the *HST*, VLA, and CXO data to a common astrometric reference frame defined by the 2MASS catalog[14], which has typical source positions accurate to $\lesssim 0\farcs1$. More accurate astrometric registration can be achieved by using the mean registration from multiple sources. Before such registration, the absolute positional accuracy of source coordinates are $\sim 1''$, $\sim 0.1''$, and $\sim 0.5''$, for the *HST*, VLA, and CXO observations, respectively.

All *HST* images were co-aligned to an archival WFPC2 F814W image of Henize 2-10 placed on the WF3 chip (P.I. Calzetti) using the bright stellar clusters common to each image. Although the WFPC2/WF3 F814W image has a lower resolution than the ACS/HRC F814W image shown in Figures 2 and 3, its larger field of view is needed to match four point sources located outside of Henize 2-10 with 2MASS sources. This produced an absolute registration accuracy of $\sim 0\farcs05$ in RA and $\sim 0\farcs04$ in Dec. Since the radio continuum VLA images have no overlap with 2MASS sources, but have features in common with the *HST* Paα image, we used this newly registered image to determine that the VLA images required an astrometric shift of $\sim 0\farcs08$ west and $\sim 0\farcs10$ north, which is reasonable given the absolute astrometric accuracy of the VLA alone. We note that the central non-thermal radio source was not used in the astrometric registration procedure and that the Paα and Hα counterparts to the radio source were discovered after the image registration. Applying these shifts to the original VLA coordinates of the central non-thermal source, we obtain a position of $08^{\rm h}36^{\rm m}15\fs117$ in RA and $-26^\circ24'34\farcs07$ in Dec.

To determine the absolute astrometry of our X-ray sources, we similarly matched the X-ray source positions against 2MASS positions, excluding the two X-ray point sources within $5''$ of the non-thermal radio source. Using five sources matched to within their 3σ positional uncertainties, we determined the absolute astrometric shift, a $\sim 0\farcs05$ shift west and $\sim 0\farcs02$ shift south of the original CXO positions. The combined statistical and systematic error of the shift is $0\farcs12$ in RA and $0\farcs33$ in Dec. Since the hard central X-ray is close to the optical axis of the CXO observation and has ~ 180 net counts, its positional error of $0\farcs13$ in RA and $0\farcs33$ in DEC is dominated by the error in absolute astrometry. The hard X-ray source, located at $08^{\rm h}36^{\rm m}15\fs114$ in RA and $-26^\circ24'33\farcs75$ in Dec, is coincident with the non-thermal radio source within the 1σ error on the CXO position.

One potential problem with registering observations taken at different wavelengths at different times is the proper motions of sources that define the reference frame (2MASS sources in this case). However, we note that this would not affect the relative astrometry between the *HST* and VLA images. Therefore, our conclusion that the central non-thermal radio source does not coincide with an optical star cluster remains secure. The same is true for our finding that the radio source is spatially coincident with a local peak in Hα and Paα emission. The main concern is the position of the central non-thermal radio source with respect to the hard X-ray source. The *Chandra* observation was taken in early 2001 and the point sources in that image that were matched to 2MASS sources ($\sim$ epoch 2000 coordinates) all have proper motions less than $\sim$25 mas yr^{-1}. Therefore, the sources defining the reference frame had not moved significantly roughly a year later when the *Chandra* observation was taken. The *HST* image (and therefore the VLA positions) that we tied to 2MASS was taken in early 2008. However, the four stars used in the registration process

have proper motions less than ∼5 mas yr^{-1} (or have no measurement). So again, it does not appear that the sources defining the reference frame had moved significantly at the time the *HST* observation was taken.

Discussion

Possible Alternative Origins for the Nuclear Source in Henize 2-10

While we have already shown (in the main paper) that a low-luminosity AGN is a natural explanation for the nuclear source in Henize 2-10, we have also considered whether the nuclear source could have an alternative origin such as one or more X-ray binaries, supernova remnants, more recently created supernovae, or some combination of these objects. A tantalizing interpretation for the morphology of the quasi-linear structure seen in ionized gas emission is outflow from the central source, for which the aforementioned phenomenon would have difficulty accounting for. However, in the discussion that follows, we simply consider the radio and X-ray luminosities of the nuclear source and disregard any possible connection to the elongated ionized gas structure. We also make use of the *ratio* of the radio to X-ray luminosities, $R_X = \nu L_\nu(5\ \mathrm{GHz})/L_X(2-10\ \mathrm{keV})$[39]. For reference, the nuclear source in Henize 2-10 has log $R_X \sim -3.6$. Typical low-luminosity AGN have log R_X between -2.8 and -3.8[21].

i. Stellar-mass black hole X-ray binaries?

While the most luminous black hole X-ray binaries may be capable of producing the observed hard X-ray emission from the nuclear source in Henize 2-10, these objects have a deficit of radio emission. Using a sample of seven Galactic black hole X-ray binaries[25], we find log $R_X < -5.3$. X-ray binaries are simply too weak in the radio to account for both the X-ray *and* radio properties of the nuclear source in Henize 2-10.

ii. Supernova Remnants?

Multiple supernova remnants could in principle account for the non-thermal radio emission coming from the nuclear source in Henize 2-10; however, these objects have relatively weak X-ray luminosities in the 2-10 keV band. Take Cas A for example, one of the most luminous Galactic supernova remnants in the radio and hard X-rays with an age of ∼300 years. At epoch 2000, Cas A had a 5 GHz luminosity[40,41] of 4.7×10^{34} erg s^{-1} and a 2-10 keV luminosity[42] of 2.6×10^{36}erg s^{-1}, giving log $R_X \sim -1.7$.

We also consider the ultraluminous supernova remnant J1228+441[43] in the Magellanic-type irregular starburst galaxy NGC 4449. At a distance of 3.8 Mpc[44], the 5 GHz luminosity[45] of this supernova remnant in 2002 was $\sim 3.4 \times 10^{35}$ erg s^{-1}. Using the 0.3-8 keV luminosity in 2001 and the model for the X-ray spectrum of J1228+441[46] we derive a 2-10 keV luminosity of $\sim 1.7 \times 10^{38}$ erg s^{-1} at 3.8 Mpc, giving log $R_X \sim -2.7$. Since even extremely radio luminous supernova remnants are relatively weak in hard X-rays, it is unlikely that they are the origin of the radio *and* X-ray emission

from the nuclear source in Henize 2-10.

iii. Young Supernovae?

Young supernovae having strong interactions with their circumstellar medium and/or a dense ISM can be extremely luminous in both radio and hard X-rays, and can even exceed the luminosities of the nuclear source in Henize 2-10 (e.g. SN 1979C[47,48], SN 1993J[49,50]). Moreover, at some times during their early evolution, their R_X values can also be similar to that of the nuclear source in Henize 2-10. At these early times, radio supenovae are extremely compact with typical sizes of $\lesssim 0.1$ pc[51,52]. Since a previous VLBI study of Henize 2-10[23] detected no sources above 0.1 mJy beam^{-1} (the 5σ detection limit) with a beam size corresponding to $\sim$0.5 pc $\times$ 0.1 pc, young supernovae with flux densities above 0.1 mJy ($\sim$ Cas A at the distance of Henize 2-10) can be ruled out as the origin of the nuclear source in Henize 2-10.

In principle, more than 15 radio supernovae with individual fluxes beneath the sensitivity limit of the VLBI observations could go undetected yet still add up to the total VLA flux of the nuclear source in Henize 2-10. However, it is extremely unlikely that more than 15 supernovae exist within our VLA beam of $\sim$24 pc $\times$ 9 pc. At these spatial scales, the most likely host for a large number of supernovae would be one or more young massive star clusters, which have typical sizes of $\sim$5 pc. For a generous supernova lifetime of 300 years (i.e. the approximate age of the supernova *remnant* Cas A), a supernova rate of 0.025 per year would be required to have a $> 1\%$ chance of there being 15 or more supernovae. This supernova rate exceeds the maximum predicted supernovae rate of a massive super star cluster of 10^6 M$_\odot$ by more than a factor of six[53]. Such a massive cluster would be optically bright; however, no clusters are observed at the location of the nuclear radio source. While it is possible that the supposed star cluster is obscured by dust, the detection of an Hα counterpart to the radio source suggests this is unlikely.

iv. Different origins for the radio and X-ray emission?

We note that the position of the hard X-ray source is also consistent (within 3σ) with nearby young super star clusters (clusters 3 & 4 from Chandar et al. 2003[54]), which are potential hosts of high mass X-ray binaries or recent supernovae. However, the relative astrometry between the VLA and *HST* images allows us to definitively rule out the association of the central radio source with these super star clusters. We therefore consider possible scenarios in which the radio and X-ray emission have different origins.

High mass X-ray binaries are a potential source of the observed hard X-ray emission, but not the radio emission. The expected number of high-mass X-ray binaries in a collection of young super star clusters can be estimated based on observations of the Antennae galaxies[55,56]. Given a total mass of 4×10^5 M$_\odot$ between the two super star clusters consistent with the position of the hard X-ray source in Henize 2-10, we expect $\sim 6.8 \times 10^{-3}$ X-ray binaries with $L_X \gtrsim 10^{37}\,\mathrm{erg\,s^{-1}}$. At the luminosity of the hard X-ray source in Henize 2-10 ($\sim 2.7 \times 10^{39}\,\mathrm{erg\,s^{-1}}$), the expected number of X-ray binaries drops to $\sim 4 \times 10^{-4}$.

A young supernova that is exceptionally weak in the radio (to be under the VLBI detection limit, see above) is another candidate for producing the hard X-ray emission without producing the radio emission. However, a comparison with the light curves of SN 1993J[50,51] indicates that a supernova with these properties (i.e. $\log R_X < -4.7$) would be extremely young ($<<$ 1 year), at an age before the radio luminosity has reached its peak. Given this short timescale, catching such a supernova is unlikely.

The radio emission from the nuclear source in Henize 2-10 could, in principle, be due to multiple supernova remnants. For example, it is possible that more than 15 supernova remnants like Cas A or more than 2 ultraluminous supernova remnants like J1228+441 (see above) could produce the equivalent radio luminosity without producing the observed hard X-ray emission. However, we find this scenario hard to reconcile with the absence of any massive star clusters within the VLA beam of $\sim$24 pc $\times$ 9 pc, since these objects are the most likely hosts for multiple supernova remnants within such a small area. As mentioned above, the detection of an Hα counterpart to the nuclear VLA source suggests extinction is unlikely to account for the lack of a visible star cluster. To illustrate this point further, we note the presence of another compact non-thermal source in Henize 2-10 that is clearly associated with the most luminous super star cluster in the galaxy (i.e. the brightest cluster in Figure 2 and cluster 1 in Chandar et al. 2003[54]). The radio emission from this other source is almost certainly due to one or more supernova remnants. In sum, while it may be possible to contrive a scenario that does not require the presence of an active nucleus in Henize 2-10, the probability of such a scenario is exceedingly low. A low-luminosity AGN is the most natural explanation for the nuclear source in this dwarf galaxy.

Eddington Ratio of the Low-Luminosity AGN

Here we consider the accretion power of the low-luminosity AGN in Henize 2-10. For an X-ray luminosity of 2.7×10^{39} erg s^{-1} in the 2-10 keV band, the Eddington Ratio is given by $\sim 10^{-4} \times (\kappa/10) \times (2 \times 10^6\ \mathrm{M}_\odot/M_{\rm BH})$, where $\kappa = L_{\rm bol}/L_{\rm X}$ is the 2-10 keV X-ray bolometric correction[57] and $M_{\rm BH}$ is the mass of the black hole in solar masses. Using our best estimate of the black hole mass, $M_{\rm BH} = 2 \times 10^6\ \mathrm{M}_\odot$, and $\kappa = 10$, the Eddington ratio for the black hole in Henize 2-10 is $\sim 10^{-4}$. This value is uncertain by a factor of ~ 10 given the error of $\sim$1 dex in mass. The black hole in Henize 2-10 is currently radiating significantly below its Eddington limit.

Supplementary Table 1. Observations of Henize 2-10

Telescope	Description
VLA	C-band (6.2 cm, 4.9 GHz) radio continuum
VLA	X-band (3.5 cm, 8.5 GHz) radio continuum
HST	NICMOS F205W, $\sim K$-band (2.1 μm)
HST	NICMOS F190N, Paα continuum (1.9 μm)
HST	NICMOS F187N, Paα line (1.87 μm)
HST	ACS F814W, $\sim I$-band (0.8 μm)
HST	WFPC2 F658N, Hα line (0.6 μm)
HST	ACS F330W, $\sim U$-band (0.3 μm)
Chandra	ACIS, 0.5-10 keV

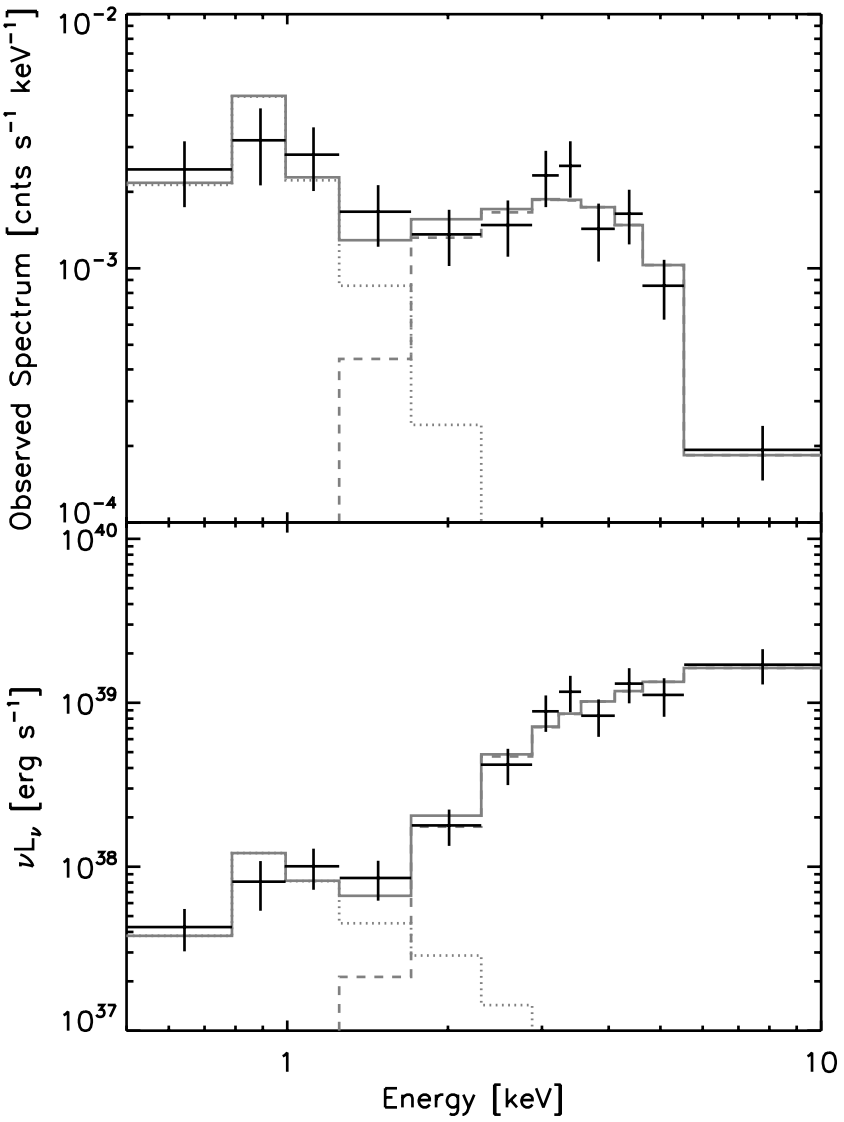

Supplementary Figure 1 - CXO spectrum of the nuclear source in Henize 2-10. The top panel displays the observed spectrum with 1σ standard deviation errors, normalized to the exposure of the observation. Despite lower effective areas at harder energies ($\gtrsim 2$ keV), the majority of photons are hard. The best-fit model, after having been folded through the instrumental response, is displayed in grey with dotted, dashed, and solid lines indicating the soft diffuse gas component, absorbed hard power-law component, and their sum, respectively. In the bottom panel we display the spectrum and best-fit model as observed νL_ν, assuming the distance to Henize 2-10. Note that the conversion to νL_ν is model dependent and the effects of neither intrinsic nor Galactic absorption have been removed. The hard power-law component dominates the total power of the source.

References

31. Ott, J., Walter, F. & Brinks, E. A Chandra X-ray survey of nearby dwarf starburst galaxies - I. Data reduction and results. *Mon. Not. Roy. Astron. Soc.* **358**, 1423-1452 (2005)

32. Fruscione, A et al. CIAO: Chandra's data analysis system. Soc. Photo. Instr. Eng. **6270** (2006)

33. Broos, P. S., et al. Innovations in the Analysis of Chandra-ACIS Observations. *Astrophys. J.* **714**, 1582-1605 (2010)

34. Kim, M., et al. Chandra Multiwavelength Project X-Ray Point Source Catalog. *Astrophys. J. Supp.* **169**, 401-429 (2007)

35. Cash, W. Parameter estimation in astronomy through application of the likelihood ratio. *Astrophys. J.* **229**, 939-947 (1979)

36. Wilms, J. & Allen, A. & McCray, R. On the Absorption of X-Rays in the Interstellar Medium. *Astrophys. J.* **542**, 914-924 (2000)

37. Verner, D. A., Ferland, G. J., Korista, K. T. & Yakovlev, D. G. Atomic Data for Astrophysics. II. New Analytic FITS for Photoionization Cross Sections of Atoms and Ions. *Astrophys. J.* **465**, 487 (1996)

38. Dickey, J. M. & Lockman, F. J. H I in the Galaxy. *Ann. Rev. Astron. Astrophys.* **28**, 215-261 (1990)

39. Terashima Y. & Wilson, A. S. Chandra Snapshot Observations of Low-Luminosity Active Galactic Nuclei with a Compact Radio Source. *Astrophys. J.* **583**, 145-158 (2003)

40. Baars, J. W. M, Genzel, R., Pauliny-Toth,I. I. K & Witzel, A. The absolute spectrum of CAS A - an accurate flux density scale and a set of secondary calibrators. *Astron. Astrophys.* **61**, 99-106 (1977)

41. Reed, J. E., Hester, J. J., Fabian, A. C. & Winkler, P. F. The Three-dimensional Structure of the Cassiopeia A Supernova Remnant. I. The Spherical Shell. *Astrophys. J.* **440**, 706 (1995)

42. Chandra Supernova Remnant Catalog. *http://hea-www.harvard.edu/ChandraSNR/G111.7-02.1* (2010)

43. Seaquist, E. R. & Bignell, R. C. Radio emission from a possible supernova remnant in the galaxy NGC 4449. *Astrophys. J.* **226**, L5-L6 (1978)

44. Annilbali, F. et al. Starbursts in the Local Universe: New Hubble Space Telescope Advanced Camera for Surveys Observations of the Irregular Galaxy NGC 4449. *Astron. J.* **135**, 1900-1916 (2008)

45. Lacey, C. K., Goss, W. M. & Mizouni, L. K. VLA Observations of J1228+441, A Luminous Supernova Remnant in NGC 4449. *Astron. J.* **133**, 2156-2162 (2007)

46. Summers, L. K., Stevens, I. R., Strickland, D. K. & Heckman, T. M. Chandra observation of NGC 4449: analysis of the X-ray emission from a dwarf starburst galaxy. *Mon. Not. Roy. Astron. Soc.* **342**, 690-708 (2003)

47. Bartel, N. & Bietenholz, M. F. Shell Revealed in SN 1979C. *Astrophys. J.* **682**, 1065-1069 (2008)

48. Immler, S., et al. Late-Time X-Ray, UV, and Optical Monitoring of Supernova 1979C. *Astrophys. J.* **632**, 283-293 (2005)

49. van Dyk, S. D., Weiler, K. W., Sramek, R. A., Rupen, M. P. SN 1993J: The early radio emission and evidence for a changing presupernova mass-loss rate. *Astrophys. J.* **432**, L115-L118 (1994)

50. Chandra, P., Dwarkadas, V. V., Ray, A., Immler, S., & Pooley, D. X-rays from the Explosion Site: 15 Years of Light Curves of SN 1993J. *Astrophys. J.* **699**, 388-399 (2009)

51. Bartel, N., et al. SN 1993J VLBI. II. Related Changes of the Deceleration, Flux Density Decay, and Spectrum. *Astrophys. J.* **581**, 404-426 (2002)

52. Ulvestad, J. S. Radio Emission from Young Supernovae and Supernova Remnants in Arp 299. *Astron. J.* **138**, 1529-1538 (2009)

53. Leitherer, C., et al. Starburst99: Synthesis Models for Galaxies with Active Star Formation. *Astrophys. J. Supp.* **123**, 3-40 (1999)

54. Chandar, R., Leitherer, C., Tremonti, C. & Calzetti, D. The Stellar Content of Henize 2-10 from Space Telescope Imaging Spectrograph Ultraviolet Spectroscopy. *Astrophys. J.* **586**, 939-958 (2003)

55. Clark, D. et al. A First Estimate of the X-Ray Binary Frequency as a Function of Star Cluster Mass in a Single Galactic System. *Astrophys. J.* **678**, 798-803 (2008)

56. Clark, D. et al. Multiwavelength Study of Chandra X-ray Sources in the Antennae. *arXiv:1008.1064* (2010)

57. Vasudevan, R. V., & Fabian, A. C. Simultaneous X-ray/optical/UV snapshots of active galactic nuclei from XMM-Newton: spectral energy distributions for the reverberation mapped sample. *Mon. Not. Roy. Astron. Soc.* **392**, 1124-1140 (2009)